Electrochemical Behaviour of Carbon Anodes Produced with Different Mixing Temperatures and Baking Levels—A Laboratory Study

Camilla Sommerseth, Rebecca Jayne Thorne, Wojciech Gebarowski, Arne Petter Ratvik, Stein Rørvik, Hogne Linga, Lorentz Petter Lossius, and Ann Mari Svensson

Abstract

Anodes fabricated from a single source coke were used for investigations of effect of porosity and surface roughness on the electrochemical performance in laboratory scale cells. In order to fabricate anodes differing in porosity, the production parameters were varied with two levels of mixing temperatures (150 and 210 °C) and three baking levels (underbaking at 1150°E, normal baking at 1260°E, overbaking at 1350°E). °E denotes the equivalent temperature which is a function of both the temperature the anode sees, and the time kept at this temperature. The low mixing anodes were more inhomogeneous with respect to both micro- and macroporosity, which can be attributed to the wetting between pitch and coke. After electrolysis, the real surface area of the low mixing anodes was about 13% higher than the high mixing anodes. Also, the low mixing electrodes had slightly larger electrochemically active surface area after electrolysis compared to the high mixing electrodes, as evidenced by higher capacitance measured at low current densities. Still, the mixing and equivalent baking temperatures did not affect the electrochemical overpotential at 1 A/cm^2 to any significant extent. This could be understood from the 3D computed tomography images, which also showed that the electrolyte does not generally penetrate into the pores on the surface, penetration will depend on the size and shape of the pore.

Keywords

Anode • Mixing temperature • Baking level • Porosity • Electrochemical performance

Introduction

High quality anodes are crucial for maintaining stable production conditions in the electrolysis cells. The industry is typically aiming for high density anodes, since low density result in reduced electrical conductivity, reduced resistance to crack propagation and thermal shock, shorter consumption time, as well as increased CO_2 reactivity [1, 2]. Furthermore, since the industry has moved towards increasing amperage in aluminium plants and increasing current density, the need for good quality anodes with a high apparent density is evident [1]. On the other hand, a lower electrochemical overpotential would be expected for electrodes that are less dense, i.e. with a higher porosity and higher surface roughness. Systematic investigations of electrochemical activity with respect to anode density/porosity/permeability are scarce in the open literature. In a previous study, the overpotential did not seem to correlate with the density of anodes, only for the most dense anode (obtained at a high baking temperature), the overpotential was slightly lower [3]. No clear correlation was found between the electrochemically active surface area (as represented by the capacitance) and the apparent density of the anodes [3]. In Ref. [4], anodes of different porosities were investigated, and the more porous anodes (i.e. pore size > 7.5 µm) were suggested to be electrochemically more active.

The first step when producing anodes is to mix coke, butts and pitch; anodes are then formed and finally baked at an elevated temperature. The mixing stage is the most

C. Sommerseth · R. J. Thorne · W. Gebarowski
A. M. Svensson (✉)
Norwegian University of Science and Technology,
Materials Science and Engineering, 7491 Trondheim, Norway
e-mail: annmari.svensson@ntnu.no

C. Sommerseth · A. P. Ratvik · S. Rørvik
SINTEF Materials and Chemistry, 7465 Trondheim, Norway

R. J. Thorne
Norwegian Institute for Air Research, 2027 Kjeller, Norway

W. Gebarowski
AGH University of Science and Technology,
30-059 Krakow, Poland

H. Linga · L. P. Lossius
Hydro Aluminium aS, 6881 Årdal, Norway

C. Chesonis (ed.), *Light Metals 2019*, The Minerals, Metals & Materials Series,
https://doi.org/10.1007/978-3-030-05864-7_161

critical step of the three production stages, as the initial interaction between coke and pitch has been shown to determine the final properties of the anode [5, 6]. In industry, a common procedure is to mix the pitch binder and the calcined petroleum coke at a temperature approximately 60 °C above the softening point of the specific pitch used [2]. It has been shown that a temperature higher than +50 °C above the pitch softening point may improve the wetting [6], and thereby better coke-pitch interactions are achieved. At higher mixing temperatures, the viscosity of the pitch will be lower and the wetting and spreading of the pitch on the coke is improved [6, 7].

In this study, anodes were made at very low and very high mixing temperature, and very low, medium and very high baking temperatures, to get a wide range of properties for the density and porosity, thereby achieving different grades of porosity and surface roughness. The main purpose of making these differing anodes was to better understand the electrochemical performance of fabricated anodes by combining electrochemical techniques with studies of the evolution of the roughness of the anode surface, and the anode-electrolyte interaction. Optical spectroscopy and computed tomography were applied for the latter. Electrochemical techniques were applied for the determination of the polarization resistance and the overvoltage, as well as the electrochemically active surface area.

Materials and Methods

Pilot Anode Materials and Electrolyte

Pilot scale anodes (Ø = 130 mm, h = 180 mm) were produced by Hydro Aluminium from a single source industrial sponge type petroleum coke of anisotropic character and an industrial grade coal tar pitch. The particle size of the aggregate was 0–2 mm to ensure a fairly homogeneous surface of the exposed anode area in laboratory scale experiments. The recipe for producing the anodes was the same throughout the series and was based on combining 1–2, 0–1 mm and a ball mill dust fraction.

The pitch binder used for production of the pilot anodes had a Mettler softening point of 119.1 °C and a QI level of 7.8%. As described above, normally a mixing temperature of 180 °C would be used for regular mixing, however, to make anodes with more extreme properties, a very low mixing temperature of 150 °C and a very high mixing temperature of 210 °C were used, termed low mixing (LM) and high mixing (HM), respectively. Three different baking levels were used corresponding to underbaking, normal baking and overbaking. The corresponding equivalent temperatures were 1150°E (low baking, LB), 1260°E (medium target baking, MB) and 1350°E (high baking (HB) (see Ref. [8] for the definition of equivalent baking temperature, °E). A graphite material from Svensk Specialgrafit AB (Ultrapure grade CMG) was used for comparison of the electrochemical performance.

The electrolyte was a cryolitic melt with a molar ratio of NaF to AlF_3 of 2.3, saturated in aluminium oxide. The cryolite was a standard cryolite from Sigma Aldrich (>97% purity) with an excess of AlF_3 of 9.8 wt% (industrial grade, sublimed in-house) and 9.4 wt% γ-Al_2O_3 from Merck. Lab-scale electrolysis experiments were performed at 1000 °C.

Anode Properties

For the experimental design, six combinations of the two mixing temperatures and the three baking levels were used during anode preparation. The coding of the anode samples is shown together with selected anode properties in Table 1.

Porosity Characterisation

An optical microscope was used to determine the porosity. 10 mm core anode samples were mounted in epoxy resin under vacuum (Epofix two-component epoxy with Epodye green fluorescent dye from Struers, Denmark). When set, samples were ground and polished stepwise down to 1 µm and studied in an optical microscope. A selective filter that only included wavelengths equal to blue light or shorter was

Table 1 Properties of the anodes [9]

Anode	Mix	Bake	T_{mix} (°C)	T_{baking} (°C)	SER (µΩm)	Permeability (nPm)	Density (g/cm^3)
LM-LB-A	L	L	150	1150	73.4	6.88	1.502
LM-LB-B	L	L	150	1150	64.3	4.09	1.552
LM-MB	L	M	150	1260	65.1	5.31	1.526
LM-HB	L	H	150	1350	60.4	3.18	1.554
HM-LB	H	L	210	1150	60.3	1.27	1.584
HM-MB	H	M	210	1260	59.7	1.40	1.576
HM-HB	H	B	210	1350	57.4	1.66	1.598

used. Fluorescent light was produced when using this filter (named B5). The magnification was ×100. Custom written macros to the NIH image software were used [10].

X-Ray Computed Tomography

3D images of anodes were obtained by X-ray computed tomography (CT), see Ref. [11] for further details. The anodes were scanned before and after electrolysis at 1.0 A/cm^2 for 1800 s.

Confocal Microscopy for Surface Analysis

A simple rod-shaped anode assembly was used for surface roughness investigations. Cores of 10 mm were drilled from the pilot anodes and the horizontal surface area was ground step-wise down to P#4000 using SiC paper. The horizontal circular surface area was investigated in terms of surface roughness using a confocal microscope (Infinitefocus from Alicona 3D). The instrument measured projected surface area and true area by including the area in voids and pores. The resolution was 410 nm and the total area scanned was 0.785 cm^2. Electrolysis was performed on the samples in an electrolyte with the same composition as previously described, for 25 min at 1.0 A/cm^2. After electrolysis, the remaining electrolyte on the anode surface was removed in a solution saturated in $AlCl_3$ and the surface roughness was determined again.

Electrochemical Measurements

All electrochemical tests were performed using a Zahner IM6 potentiostat with built-in electrochemical impedance spectroscopy (EIS) module. A PP201 20 A booster from Zahner-Elektrik was also used.

The anodes were tested electrochemically by chronopotentiometry, linear sweep voltammetry and EIS. In all electrochemical experiments, the carbon anode was the working electrode, the graphite crucible walls acted as the counter electrode and potentials were measured towards an in-house produced aluminium reference electrode, consisting of a cylindrical boron nitride container with molten aluminium in the bottom. The aluminium is in electrolytic contact with the electrolyte through a small hole, and electronically connected by a tungsten wire. All measured potentials are quoted with respect to aluminium. The anode setup and laboratory electrochemical cell used are shown in Fig. 1. The vertical anode setup is designed to minimise bubble noise from CO_2 gas formed during electrolysis, as previously shown [12]. Then chronopotentiometry was performed at 1.0 A/cm^2 for 200 s and the voltage output reported below is the average of the potential response for the last 50 s. The potential has then been IR corrected using the series resistance, R_S, obtained by EIS at open circuit potential (OCP) and extracted from Nyquist plots (i.e. Z_{Re} at intercept when Z_{Im} is zero).

EIS spectra were collected for the anode materials at an applied voltage of 1.5 V (non-IR corrected) and an amplitude of 50 mV in the frequency range 100 kHz–0.1 Hz.

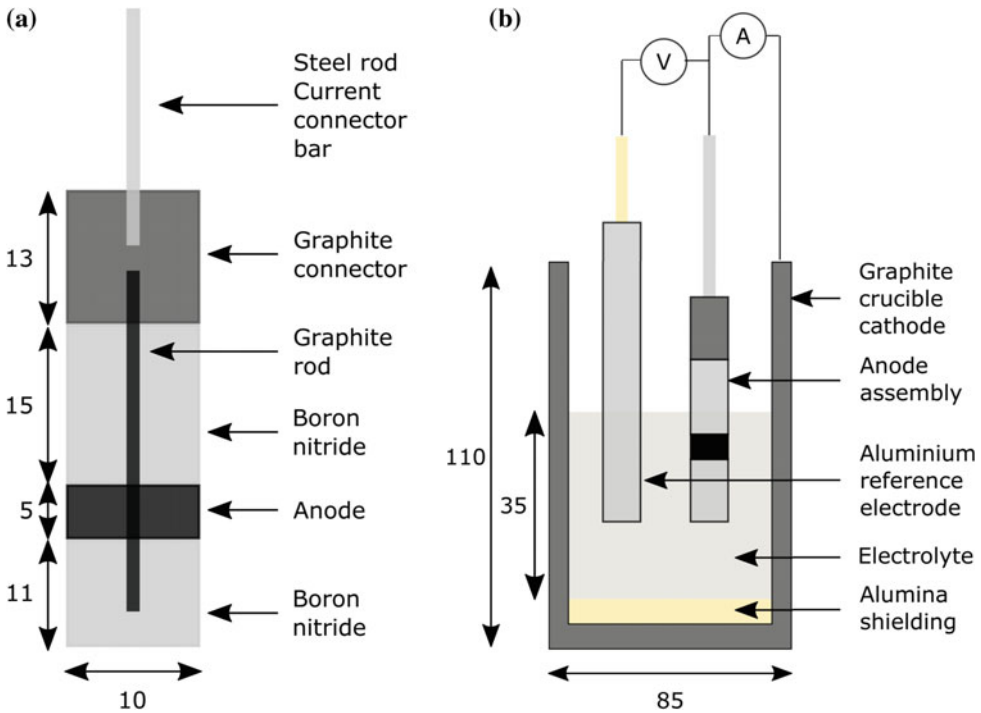

Fig. 1 Electrochemical experimental setup used when electrolysing samples for CT scanning and during general electrochemical testing. All measures are in mm. **a** Vertical anode assembly. **b** A principle sketch of the laboratory scale electrolysis cell

The EIS spectra were fitted to the LR(Q(R(LR))) circuit as described by Harrington and Conway [13], except that the ideal double layer capacitance, C_{dl}, has been replaced by a constant phase element, Q (or often denoted as CPE) to account for the roughness of the anodes. The equivalent circuit was derived for a general reaction sequence involving intermediately adsorbed species [13]. The LR(Q(R(LR))) circuit was used to extract C_{dl} indirectly by approximating the effective capacitance of the surface (C_{eff}) using Eq. 1 below (same as Eq. 15 in Orazem et al. [14], developed for Faradaic systems).

$$C_{eff} = Q^{1/a}\left(\frac{R_S(R_{CT1}+R_{CT2})}{R_S+R_{CT1}+R_{CT2}}\right)^{\frac{1-\alpha}{\alpha}} \quad (1)$$

In Eq. 1, R_S, R_{CT1} and R_{CT2} are the series resistance, the first charge-transfer resistance and the second charge-transfer resistance, respectively. α is the dimensionless constant phase element exponent.

Results and Discussion

The porosity distribution in the anodes was measured by optical microscopy. Figure 2 shows the amount of open porosity in the anodes versus diameter of the pores found by optical microscopy. The porosity peaks at 15 µm correspond to pores between fines. The peaks at 30–100 µm correspond to calcination pores, appearing when volatiles are being released from pitch during baking and larger pores between fines. The peaks at about 200–600 µm are much more evident for the low mixing temperature anodes, compared with the high mixing temperature anodes. Thus, it seems reasonable to conclude that these pores are related to poor wetting between pitch and coke due to too low mixing temperatures, which result in inhomogeneous anodes.

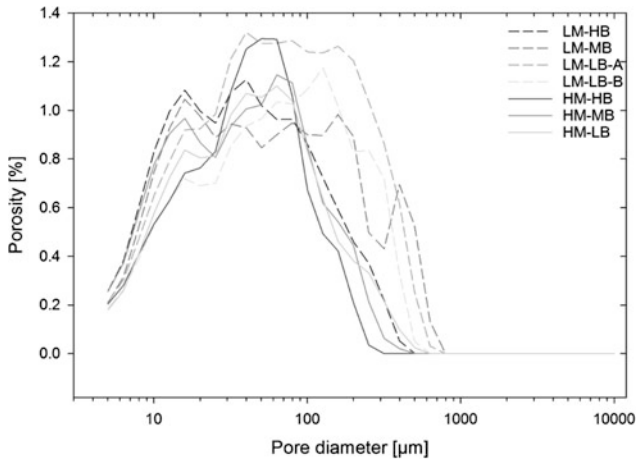

Fig. 2 Porosity versus pore diameter size obtained by optical microscopy. The results are averages between two or four parallels

The effects of mixing and baking temperature on the internal morphology of the anodes were studied by X-ray computed tomography (CT), and images of some selected anodes varying in baking level and mixing temperature are shown in Fig. 3. The images show the same cross-sections of the interior of the anodes before and after electrolysis for 1.0 A/cm^2 for 30 min.

The anode samples were hot-pulled from the electrolyte with current still on and quickly cooled. This was done to create a frozen image of what the anode and electrolyte looked like during electrolysis. The tomographs show the non-electrolysed sample along with the same sample after electrolysis and at the same rotation. The high-density disk in the middle of each sample is the graphite current connector rod as described in Fig. 1a. In general, it can be seen that the network of open porosity in the low mixing temperature anodes is noticeably higher than the high mixing temperature anode. The low mixing temperature anodes have larger and more connected pores compared to the high mixing temperature anodes. These larger pores are also evident in the aforementioned porosity analysis (Fig. 2). The high mixing temperature anode is more homogeneous and the pores present are much smaller and not as interlinked. CT clearly shows qualitatively how the density, and then parameters like SER and permeability are improved with a more optimised mixing temperature as already argued in several studies [1, 15, 16]. The larger pores in the low mixing temperature anodes are formed when coke particles are not well wetted with pitch. This is supported by the observation of pore walls appearing very rough for the low mixing temperature anodes. When the coke and pitch interactions are good, the pore walls are smooth. This can clearly be seen in Fig. 3.

From the CT images of anode LM-MB (Fig. 3b) it can be seen that highly porous coke grains, so-called "bubble coke" [11], tend to protrude from the matrix after electrolysis, indicating that it is consumed at a lower rate than the regular coke grains. This is most likely due to higher electrical resistivity through these high porosity grains. Alternatively, it might be related to poor electrolyte wetting on these coke grains. In the same image it is evident that electrolyte does not penetrate into a large, open pore as seen to the right of the image. This finding was to a large extent confirmed in other CT images of this data set, not displayed in this paper. Many pores do not show any or only slight penetration of electrolyte. In Ref. [11] it is shown that the pores have to be very large and/or of a convex character in order for the electrolyte to penetrate. This is most likely related to CO_2 gas bubbles from the electrolytic reaction occupying the pores volumes, and thus preventing the penetration by the electrolyte.

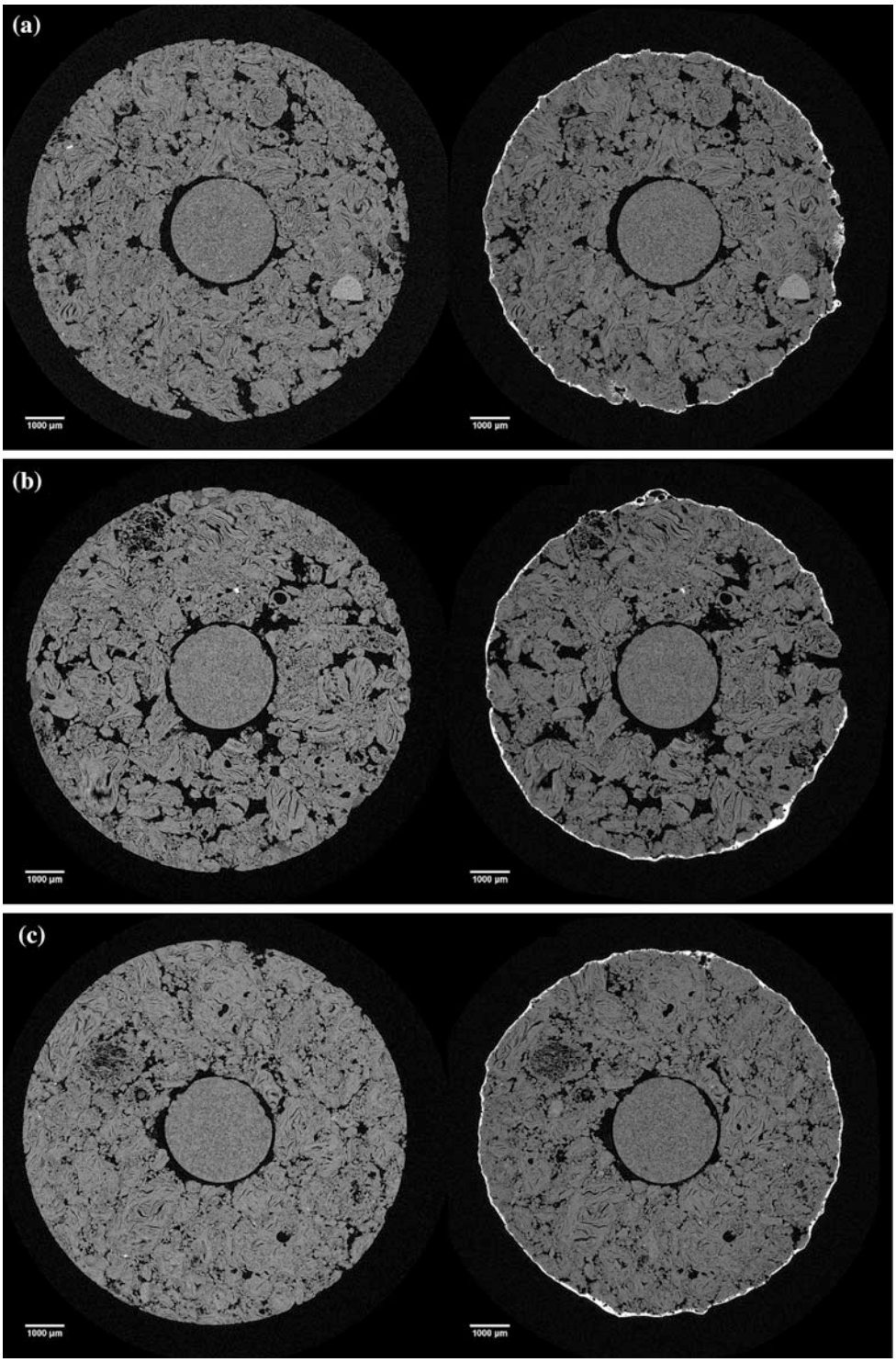

Fig. 3 CT images of an interior cross-section of some selected anodes before (left) and after (right) electrolysis. **a** Anode LM-LB-B, **b** Anode LM-MB and **c** Anode HM-HB

Confocal microscopy was used to determine the ratio of true area over projected area (geometric 2D area) (TA/PA) for all the anodes varying in baking and mixing temperature. The results are shown in Fig. 4. Circle points show TA/PA on the same anode samples after they had been electrolysed for 25 min at 1.0 A/cm^2. The higher value of the true area/projected area measurement of the HM-HB sample after electrolysis is considered anomaly.

An increase of TA/PA of about 40% is seen for the anodes after electrolysis compared to the polished, non-electrolysed samples. This is in good agreement with Jarek and Thonstad [3], who found by impedance

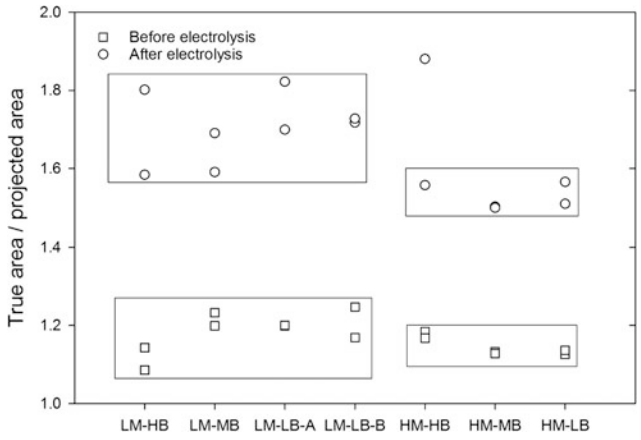

Fig. 4 Ratio of true area over projected area obtained by confocal microscopy on freshly cut and ground samples and electrolysed samples (circles) at 1.0 A/cm^2 for 25 min. The low and high mixing temperature anodes have been "boxed" together

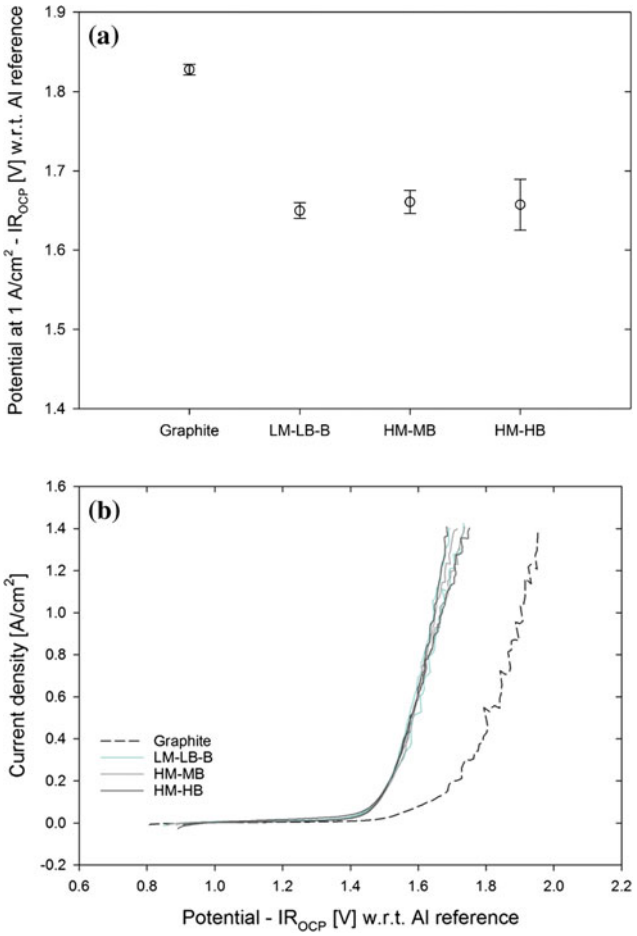

Fig. 5 **a** Chronopotentiometry measurements at 1.0 A/cm^2. Graphite was used as anode reference material. **b** IR corrected polarisation curves for the same anodes

measurements before and after electrolysis an increase in double layer capacitance of 45%. These experiments were performed on anode samples that had a well-defined flat anode area, shielded by boron nitride. The samples were also tilted (about 120° compared to a horizontal setup) to facilitate gas bubble release. From CT images (Fig. 3) it can also be seen qualitatively that the electrolysed surfaces are rougher than the non-electrolysed samples.

The increased number of pores in the low mixing anodes are expected to influence the electrochemical active surface area somewhat. However, as seen from the CT images, even large pores are not filled with electrolyte, implying that geometric surface area is not directly linked to the electrochemical active surface area. The removal of electrolyte by soaking in $AlCl_3$ is a weak point of this experiment, as the removal might either be incomplete, or there is a risk of detaching small pieces of carbon. However, we do not believe that the removal step affects the main observations here.

Figure 5a shows results from chronopotentiometry at 1.0 A/cm^2 measured for graphite and anodes LM-LB-B, HM-MB and HM-HB. Chronopotentiometry was performed on two parallel samples of each anode quality in the same melt on the same day. Figure 5b shows the second forward polarisation curves out of three consecutive forward and backward scans with a slow sweep rate of 0.1 V/s for the same anodes as shown in Fig. 4a.

No large differences in potential output can be seen between the anodes varying in baking and mixing temperatures, and hence varying in apparent density (1.50–1.59 g/cm^3) and porosity in Fig. 5. Jarek and Orman [17] found that overpotential increased with decreasing porosity. However, this was when comparing graphite to baked carbon anodes. The current work also shows increased overpotential for graphite samples compared with the baked carbon anodes, however, no significant differences can be seen between the baked carbon anodes. Jarek and Thonstad [3] found that the anodic overpotential on carbon anodes decreased slightly with increasing apparent density. In their work the apparent density ranged from 1.32 to 1.61 g/cm^3, which was a wider range and gives more extreme porosity ranges compared to the present work.

The EIS data obtained at 1.5 V (non-IR corrected) was fitted with an LR(Q(R(LR))) circuit. The values obtained for the effective capacitance, C_{eff} and C_{eff} divided by the average true area over projected area numbers are shown in Fig. 6 for selected anodes.

The effective capacitance was calculated from Eq. 1, and divided by the geometric area of the anode (1.52 cm^2). The recorded current density response varied a little between each EIS scan, due to small variations in the ohmic potential drop, but these variations are too small to affect the potential output to a large extent.

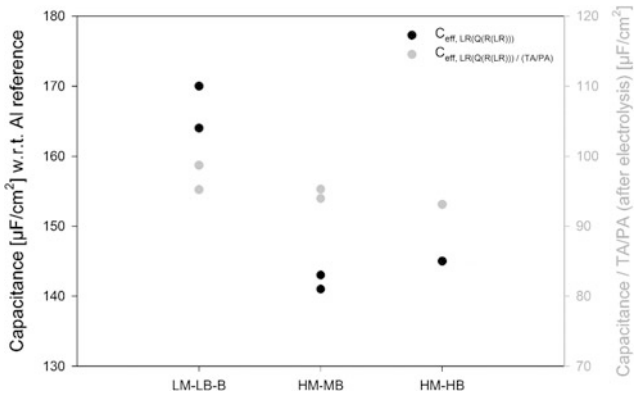

Fig. 6 Effective capacitance determined from EIS spectra for selected anodes

The effective capacitance values, C_{eff}, shown are fairly consistent with the values found by Thonstad [18]. Nevertheless, it is evident that the LM anodes have a higher C_{eff} than the HM anodes. This is due to the increased surface area of the more porous LM anode. The increase of C_{eff} from the LM anodes to the HM anodes is approximately 16%. The difference of true area over projected area measured by confocal microscopy between the LM and the HM anodes after electrolysis was about 13%. Hence, the effective capacitance and the TA/PA measurements are in good agreement. Since the coke and pitch materials are the same throughout the entire anode series it is expected that the C_{eff} over true area/projected area numbers are approximately the same. This proves that although the larger pores are not filled with electrolyte (Fig. 3b), the increase in the surface roughness contributes to an increased electrochemically active area. The increased active surface area, however, does appear to lower the overpotential for these electrodes significantly (Fig. 5). One explanation can be the lower current density during the EIS measurements compared to the current density before CT imaging: ≈0.1 A/cm^2 versus 1 A/cm^2. The lower current density will give a very low CO_2-evolution at the anode. The low gas evolution may not be enough to prevent electrolyte penetration into the pores. The lower potential (and hence responding current density) chosen during the EIS measurements was indeed because of reduction in gas bubble noise in the electrochemical measurement.

Conclusions

Anodes differing in porosity were obtained by using a very low (150 °C) and a very high (210 °C) mixing temperature, at three different equivalent baking levels (1150, 1260 and 1350°E). The anodes were characterized with respect to porosity, surface roughness and electrochemical performance (reaction overpotential and capacitance). As expected, a non-ideal low mixing temperature is highly detrimental to the density of the anode. CT images showed that the low mixing anodes were non-homogeneous, with many large pores distributed unevenly throughout the anode sample, most likely a result of insufficient wetting of the pitch. The high mixing anodes were more homogeneous. An increase in geometric surface area of about 40% was observed between non-electrolysed samples and electrolysed samples. With confocal microscopy it was shown that the real surface area of the low mixing anodes was about 13% higher than the high mixing anodes after electrolysis. The low mixing electrodes had slightly higher capacitance values after electrolysis compared to the high mixing electrodes, indicating also a correspondingly larger electrochemically active surface area. However, the density and porosity did not affect the electrochemical overpotential to any significant extent. This could be understood by the CT images, which also showed that the electrolyte does not generally penetrate the pores on the surface, penetration will depend on the size and shape of the pore. Thus, the higher surface area of the less dense anodes does not significantly reduce the overpotential.

Acknowledgements The work was financed by Hydro Aluminium and The Research Council of Norway through the research program called "HAL Ultra Performance Aluminium Cell". Thanks are due to Aksel Alstad at the NTNU workshop for fabricating the experimental parts, Cristian Torres Rodriguez, technicians at Hydro Aluminium Årdalstangen, Ole Tore Buset and Jannicke Kvello for help with various experimental techniques.

References

1. S. Wilkening (2009) Maintaining Consistent Anode Density Using Varying Carbon Raw Materials. In: *Light Metals* 2009, The Minerals, Metals & Materials Society, Pittsburgh; Springer, New York, p 991–997.
2. D. Kocaefe, A. Sarkar, S. Das, S. Amrani, D. Bhattacharyay, D. Sarkar and Y. Kocaefe (2013) Review of Different Techniques to Study the Interactions between Coke and Pitch in Anode Manufacturing. In: *Light Metals 2013*, The Minerals, Metals & Materials Society, Pittsburgh; Springer, New York 1045–1050.
3. S. Jarek and J. Thonstad (1987) Double-layer capacitance and polarization potential of baked carbon anodes in cryolite-alumina melts. *J. Appl. Electrochem.* 17:1203–1212.
4. S. Zuca, C. Hederlicka and M. Terzi (1980) On Porosity-Overvoltage Correlation for Carbon Anodes in Cryolite-Alumina Melts. Electrochim. Acta, 25:211–216.
5. V. Rocha, C. Blanco, R. Santamaría, E. Diestre, R. Menéndez and M. Granda (2007) An Insight into Pitch/Substrate Wetting Behavior. The Effect of the Substrate Processing Temperature on Pitch Wetting Capacity. *Fuel* 86:1046–1052.
6. A. Sarkar, D. Kocaefe, Y. Koceafe, D. Sarkar, D. Bhattacharyay, B. Morais and J. Chabot (2014) Coke-pitch Interactions during Anode Preparation. *Fuel* 117:598–607.

7. A. Mirchi, G. Savard, J. Tremblay and M. Simard (2002) Alcan Characterization of Pitch Performance of Pitch Binder Evaluation and Process Changes in an Aluminium Smelter. In: *Light Metals* 2002, The Minerals, Metals & Materials Society, Pittsburgh; Springer, New York, p 525–533.
8. L.P. Lossius, I. Holden and H. Linga (2006) The Equivalent Temperature Method for Measuring the Bakin Level of Anodes. In: *Light Metals 2006*, The Minerals, Metals & Materials Society, Pittsburgh; Springer, New York p 609–613.
9. C. Sommerseth (2016) *The Effect of Production Parameters on the Performance of Carbon Anodes for Aluminium Production*. Ph.D. thesis, Norwegian University of Science and Technology.
10. S. Rørvik and H. Øye (1996) A Method for Characterization of Anode Pore Structure by Image Analysis. In: *Light Metals 1996*, The Minerals, Metals & Materials Society, Pittsburgh; Springer, New York p 561–568.
11. C. Sommerseth, R. Thorne, S. Rørvik, E. Sandnes, A. Ratvik, L. Lossius, H. Linga and A. Svensson (2015) Spatial Methods for Characterising Anodes for Aluminum Production. In: *Light Metals 2015*, The Minerals, Metals & Materials Society, Pittsburgh; Springer, New York p 1141–1146.
12. R. Thorne, C. Sommerseth, A. Ratvik, E. Sandnes, S. Rørvik, L. Lossius, H. Linga and A. Svensson (2015) Correlation between Coke Tyope, Microstructure and Anodic Reaction Overpotential in Aluminium Electrolysis. *J. Electrochem. Soc.,*162:E296–E306.
13. D. Harrington and B. Conway (1987) AC impedance of Faradaic Reactions Involving Electrosorbed Intermediates. I. Kinetic Theory. *Electrochim. Acta*, 32:1703–1712.
14. M. Orazem, I. Frateur, B. Tribollet, V. Vivier, S. Marcelin, N. Pebere, A. Bunge, E. White, D. Riemer and M. Musiani (2013) Dielectric Properties of Materials showing Constant Phase Element (CPE) Impedance Response. *J. Electrochem. Soc.*, 160: C215–C225.
15. K. Hulse, R. Perruchoud, W. Fischer and B. Welch (2000) Process Adoptions for Finer Dust Formations: Mixing and Forming. In: *Light Metals 2015*, The Minerals, Metals & Materials Society, Pittsburgh; Springer, New York p 467–472.
16. C. Sommerseth, R. Thorne, A. Ratvik, E. Sandnes, L. Lossius, H. Linga and A. Svensson (2017) The Effect of Varying Mixing Temperatures and Baking Level on the Quality of Pilot Scale Anodes—A Factorial Design Analysis. *Metals,*7:1–12.
17. S. Jarek and Z. Orman (1985) The Faradaic Impedance of the Carbon Anode in Cryolite-Alumina Melt. *Electrochim. Acta*, 30:341–345.
18. J. Thonstad (1970) The Electrode Reaction on the C, CO_2 Electrodes in the Cryolite-Alumina Melts – II. Impedance Measurements. *Electrochim. Acta*, 15:1581–1595.